remote sensing

MDPI

Article

Distribution, Magnitude, and Variability of Natural Oil Seeps in the Gulf of Mexico

Carrie O'Reilly [1,*], Mauricio Silva [1], Samira Daneshgar Asl [2], William P. Meurer [3] and Ian R. MacDonald [1]

[1] Department of Earth, Ocean, and Atmospheric Science, Florida State University, Tallahassee, FL 32306, USA; msilvaaguilera@fsu.edu (M.S.); imacdonald@fsu.edu (I.R.M.)
[2] Department of Geography, University of California, Santa Barbara, Santa Barbara, CA 93106, USA; samira@geog.ucsb.edu
[3] ExxonMobil Upstream Research Company, Spring, TX 77389, USA; william.p.meurer@exxonmobil.com
* Correspondence: clo17@fsu.edu

Abstract: The Gulf of Mexico is a hydrocarbon-rich region characterized by the presence of floating oil slicks from persistent natural hydrocarbon seeps, which are reliably captured by synthetic aperture radar (SAR) satellite imaging. Improving the state of knowledge of hydrocarbon seepage in the Gulf of Mexico improves the understanding and quantification of natural seepage rates in North America. We used data derived from SAR scenes collected over the Gulf of Mexico from 1978 to 2018 to locate oil slick origins (OSOs), cluster the OSOs into discrete seep zones, estimate the flux of individual seepage events, and calculate seep recurrence rates. In total, 1618 discrete seep zones were identified, primarily concentrated in the northern Gulf of Mexico within the Louann salt formation, with a secondary concentration in the Campeche region. The centerline method was used to estimate flux based on the drift length of the slick (centerline), the slick area, and average current and wind speeds. Flux estimates from the surface area of oil slicks varied geographically and temporally; on average, seep zones exhibited an 11% recurrence rate, suggesting possible intermittent discharge from natural seeps. The estimated average instantaneous flux for natural seeps is 9.8 mL s^{-1} (1.9×10^3 bbl yr^{-1}), with an annual discharge of 1.73–6.69 $\times 10^5$ bbl yr^{-1} (2.75–10.63 $\times 10^4$ m^3 yr^{-1}) for the entire Gulf of Mexico. The temporal variability of average flux suggests a potential decrease following 1995; however, analysis of flux in four lease blocks indicates that flux has not changed substantially over time. It is unlikely that production activities in the Gulf of Mexico impact natural seepage on a human timescale. Of the 1618 identified seep zones, 1401 are located within U.S. waters, with 70 identified as having flux and recurrence rates significantly higher than the average. Seep zones exhibiting high recurrence rates are more likely to be associated with positive seismic anomalies. Many of the methods developed for this study can be applied to SAR-detected oil slicks in other marine settings to better assess the magnitude of global hydrocarbon seepage.

Keywords: SAR imagery; oil slicks; seep zones; Gulf of Mexico; oil seepage fluxes

Citation: O'Reilly, C.; Silva, M.; Daneshgar Asl, S.; Meurer, W.P.; MacDonald, I.R. Distribution, Magnitude, and Variability of Natural Oil Seeps in the Gulf of Mexico. *Remote Sens.* **2022**, *14*, 3150. https://doi.org/10.3390/rs14133150

Academic Editor: Francesco Bignami

Received: 13 June 2022
Accepted: 28 June 2022
Published: 30 June 2022

1. Introduction

Natural hydrocarbon seeps are common on many continental margins worldwide, e.g., [1–4] (Figure 1; Table 1). Hydrocarbon-rich regions, such as the Gulf of Mexico, are characterized by the perennial presence of floating oil slicks [5], which may indicate petroleum accumulations available for commercial exploitation. Surface slicks are visible from space and are routinely detected through remote sensing methodologies, especially in satellite imagery [6,7]. Improved technology, the vast expansion of synthetic aperture radar (SAR) datasets, and the understanding of oceanographic constraints on slick occurrence allow for an updated seep distribution and flux estimate in the Gulf of Mexico.

The underlying geology of the Gulf of Mexico supports a highly productive hydrocarbon province; natural and anthropogenic oil slicks are regularly observed on the sea surface. Widespread evaporite layers, known as Louann salt, were generated during the Jurassic-age

formation of the Gulf of Mexico basin. With plate tectonism dormant, subsequent mass deposition of sediments rich in organic matter, in anoxic or suboxic environments, created conditions required for source rock, and hydrocarbon, generation. Continued sediment deposition resulted in the kinetic deformation of underlying salts; less dense salt structures pushed through overlying sediments, forming hydrocarbon migration pathways [8]. The resulting prolific natural hydrocarbon seeps serve vital roles for both the benthic ecosystem and offshore energy exploration in a highly industrialized marine region. Chemosynthetic communities are common across the Gulf's continental slope [9]. The highest average daily commercial production of oil in the Gulf of Mexico since 2000 was approximately 1.9 million bbl d^{-1} in 2019, accounting for approximately 16% of U.S. crude oil production [10]. In comparison, the current estimated total annual discharge of natural seeps in the Gulf of Mexico is 1.58–5.94 × 10^5 bbl yr^{-1} (2.5–9.4 × 10^4 m^3 yr^{-1}; [11]). This estimate relied on two assumptions: a consistent 0.1 µm slick thickness and an 8–24 h surface residence time, the latter of which will be addressed in the current study through the use of centerline slick age estimates. SAR is often used to study natural oil slicks, as well as slicks resulting from oil spills.

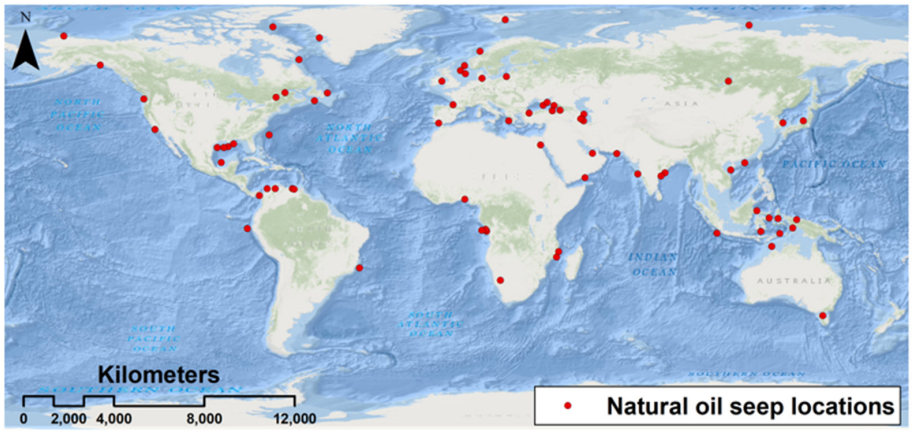

Figure 1. Generalized locations of well-documented natural oil seeps.

Table 1. Example references documenting geologic features of known oil seeps. Corresponds with seep locations in Figure 1.

Literature Reference	Location	Geologic Features	Water Depth (m)	Flux
Agirrezabala and López-Horgue, 2017 [12]	Bay of Biscay	Authigenic carbonates, diapirs		
Barberes et al., 2020 [13]	Iberian Basin	Authigenic carbonates, mud volcanoes		
Bernardo and Bartolini, 2015 [14]	Western Caribbean, Panama			
Bojesen-Koefoed et al., 2004 [15]	Baffin Bay, West Greenland			
Burns et al., 2010 [16]	Timor Sea	Carbonate domes	90	
Camplin and Hall, 2014 [17]	Indonesia/Java Sea	Pockmarks, carbonates, mounds, locally formed hydrates	1800	
Cazzini et al., 2015 [18]	Adriatic Sea, Italy	Carbonate platforms		
Chen and Hu, 2014 [19]	Cariaco Basin, Venezuela			
Coughlan et al., 2021 [20]	Irish Sea	Pockmarks, mounds, authigenic carbonates, mud diapirs	>40	
Cramer and Franke, 2005 [21]	Laptev Sea, NE Siberia	Gas hydrates		
Dill and Kaufhold, 2018 [22]	Colombia	Mud volcanoes, diapirs		

Table 1. *Cont.*

Literature Reference	Location	Geologic Features	Water Depth (m)	Flux
Dupré et al., 2015 [23]	Sea of Marmara	Carbonates, mud volcanoes, gas hydrates	Avg~600	
Feng et al., 2018 [24]	South China Sea	Carbonates, mud volcanoes, pockmarks		
Fildani et al., 2005 [25]	Talara Basin, NW Peru	Carbonates		
Foster et al., 2015 [26]	Baffin Bay, eastern Canadian Arctic			
Freire et al., 2011 [27]	Japan Sea	Gas hydrates, pockmarks, mounds	900–1100	
Freire et al., 2017 [28]	Espírito Basin, Brazil	Carbonates, salt diapirs	2700	
Gbadebo, 2010 [29]	SW Nigeria			
Hakimi et al., 2018 [30]	Gulf of Aden, south of Yemen	Carbonates		
Himmler et al., 2008 [31]	Southern Namibia	Carbonates	Onshore	
Hovland et al., 2012 [32]	North Sea	Salt diapirs, pockmarks		
Intawong et al., 2019 [33]	Mozambique Channel	Pockmarks, carbonates		
Ivanov et al., 2020 [34]	Black Sea	Mud volcanoes (Russian sector)	1000–1050	400–3000 tons yr^{-1} (Georgian sector), 140–100 tons yr^{-1} (Turkish sector)
Ivanov et al., 2020 [4]	South Caspian Sea	Mud volcanoes		
Ivanov and Gerivani, 2020 [35]	Persian Gulf, UAE	Carbonates, faults and folds, salt domes		
Jatiault et al., 2018 [36]	Lower Congo Basin, Angola	Salt tectonics, pockmarks	1200–2700	4380 m^3 yr^{-1} oil
Jauer and Budkewitsch, 2010 [37]	Labrador Sea, Canada	Mounds, mud volcanoes		
Johansen et al., 2017 [5]	Gulf of Mexico, GC600 and MC118	Salt diapirs, gas hydrates, authigenic carbonate mounds	850–1200	2.62–10.8 (oily), 62.2–101 (mixed), 188 (gas) m^3 yr^{-1}
Leifer et al., 2004 [38]	Coal Oil Point, Santa Barbara, CA	Salt diapirs, mud volcanoes, mounds, brine pools	20–70	1.5×10^5 m^3 d^{-1} gas, 80 bbl d^{-1} oil
Liira et al., 2019 [39]	Svalbard	Carbonates, pockmarks		
Logan et al., 2010 [40]	Offshore Australia	Pockmarks, carbonates		
Mitra et al., 2013 [41]	Offshore India			
Mityagina and Lavrova, 2018 [42]	Eastern Black Sea	Mud volcanoes		
Nemirovskaya and Sivkov, 2012 [43]	Baltic Sea			
Nesbitt et al., 2013 [44]	NE Pacific, Cascadia margin, WA	Cascadia accretionary wedge, carbonates		
Pinet et al., 2008 [45]	St. Lawrence Estuary, Canada	Pockmarks, seismic chimneys, carbonates	65–355	
Römer et al., 2012 [46]	Arabian Sea, offshore Pakistan	Mud volcanoes		
Römer et al., 2014 [47]	Eastern Mediterranean Sea	Authigenic carbonates, pockmarks	1000–1800	
Sakran et al., 2016 [48]	Gulf of Suez	Carbonates		
Short et al., 2007 [49]	Gulf of Alaska		41–327	
Taylor et al., 2000 [50]	Blake Ridge, offshore S. Carolina, U.S.	Pockmarks, salt diapirs		
Venkatesan et al., 2013 [51]	Alaskan Beaufort Sea			
Zakharenko et al., 2019 [52]	Lake Baikal, Russia	Gas hydrates, mud volcanoes	855–1370	
Zelilidis et al., 2015 [53]	Ionian Sea, Greece	Carbonates, diapirs		

Natural oil slicks are thin layers of oil sourced from natural seepage that visibly dampen capillary waves. Approximately 1 mL of crude oil is required to generate a 10 m^2 slick with a thickness of 0.1 µm [6]. Thicker oil slicks (>0.4 µm) display chromatic properties not visible below this threshold [54]. Oil slicks are easily detectable by satellites, specifically SAR, under all sunlight and cloud conditions [55–57], and under ideal wind conditions (2–7 m s^{-1}; [58–60]). SAR is an active form of remote sensing; the sensors transmit their own microwave signals to the Earth's surface and analyze the backscatter [61]. The viscoelastic properties and lower permittivity of oil slicks influence the degree of radar backscatter [60,62]. Oil slicks are areas of lower backscatter [63]. Oil slicks appear as a dark image anomaly in SAR scenes because the smoother ocean surface reflects radar energy away from the sensor to a greater degree than the rougher surface from unoiled water [56,61,63].

SAR imaging has been shown to reliably detect surface oil slicks emanating from persistent high-volume natural seeps, allowing researchers to identify oil slick origins (OSOs; [7]). The oil slick itself elongates and flows away from the OSO, driven by winds and surface currents [11,64]. Oil slick compositions are modified over time. As slicks age, highly volatile components are quickly lost to the atmosphere and higher-molecular-weight compounds are concentrated. Slick appearance in thicker examples will transition from thick and brown to thin and gray, with a thinning rainbow intermediate; older, thinner slicks may be more difficult to detect by SAR [65]. Although OSOs indicate the general location of the seafloor source of an oil slick, the OSO may be offset from this source because subsurface currents deflect the vertical movement of the hydrocarbons in the water column [7]. The size and rise speed of bubbles also play a role; bubbles composed primarily of oil will rise at slower speeds than those composed primarily of gas [66]. The extent of this deflection, approximately two times the water depth with a maximum deflection radius of 3500 m, was characterized for seeps found in the northern Gulf of Mexico [7]. Repeat occurrence of slicks in a given area is a probable indicator of a seep zone.

MacDonald et al. [11] identified 914 seep zones producing persistent surface slicks in the Gulf of Mexico using a neural network analysis. Seep zones are defined as fixed geologic areas that persistently produce individual or clustered OSOs from one or more localized but discrete seafloor vents. However, the delineation of a seep zone is empirical, based on the repeated detection of slicks within a discrete area that corresponds to seafloor mapping of the geologically constrained scale of venting within active seeps [67]. The identification of seep zones enhances our understanding of the subsurface geologic processes that control the distribution of oil in near-surface sediments and the release of oil into the water column and allows oil flux estimations to be calculated [11,68]. Identifying distinct seep zones based on surface slicks is difficult due to the lack of seafloor confirmation, especially since seep zones may contain many discrete vents that are active over differing timescales [64,69]. Repeated detection of surface slicks in a particular locality is a primary indicator that their source is a natural seep rather than pollution or transient phenomena [7,64]. However, in places where the number of SAR scenes is limited, low flux seeps or those with ephemeral discharge might not be detected. This study analyzed an expanded collection of satellite SAR scenes (4091) that detected natural oil slicks in the Gulf of Mexico to determine spatial and temporal trends in the distribution, abundance, and flux of active seep zones in the Gulf of Mexico.

2. Materials and Methods

2.1. Datasets

We analyzed a comprehensive dataset that encompasses the entire Gulf of Mexico, comprising interpretation from SAR data collected between 1978 and 2018. SAR data from three remote sensing vendors (MDA, Airbus, and NPA) and those previously reported by MacDonald et al. [11] were used (Table 2). Satellites used by the vendors included ERS-1, ERS-2, RADARSAT-1, ENVISAT, Sentinel-1A, and TSX-1. MacDonald et al. [11] analyzed SAR scenes collected by RADARSAT-1, JERS-1, and ERS-1 satellites. These

satellites use X-, C-, and L-band wavelengths. The combined dataset identified over 32,000 natural seep OSOs. The vendors routinely provide SAR analysis for oil companies in the form of shapefiles, with polygons representing oil slicks seen on SAR imagery and points representing OSOs (Figure 2). Oil slicks were classified by the vendors as "natural", "pollution", or of "uncertain" origin. Oil slicks classified as "pollution" and "uncertain" were filtered out of the dataset. Vendor criteria for classifying SAR anomalies as oil slicks typically include repeatability, shape, size, and location (i.e., near oil seep geologic features; [65]). The natural designation indicates that the imaged slicks exhibited characteristics that have also been observed at confirmed natural seeps. However, SAR scenes display differences in sea surface roughness and do not indicate the cause of the dampened capillary waves. In addition to oil, SAR-detected ocean surface anomalies may include spawning events, algal blooms, and wind shadowing, so ground truth analyses are required to confirm the source of the SAR-detected anomalies [70–72]. OSOs designated by the vendors and MacDonald et al. [11] as natural were compiled into one shapefile (Figure 3). MDA provided oil slick polygons that did not include OSOs. We generated OSOs for these polygons based on the shape of the features and wind direction. Both NPA and Airbus provided oil slick polygons and OSOs. In some instances, polygons were provided that represented segments of discrete seepage events. We aggregated these segments for each event, allowing us to work with a single length, area, and OSO.

Table 2. Data acquired from vendors and MacDonald et al. [11], including all classifications.

	MDA *	NPA	Airbus	MacDonald et al. [11]	Total
Years active	1997–2014	1978, 1991–2018	1992–2015	1994–2007	28
number of scenes	215	2265	1357	254	4091
number of polygons (oil slicks)	2070	29,126	7667	14,608	53,471
number of points (OSOs)	2070	29,089	3826	14,531	49,516

* OSOs were generated for the individual oil slick polygons based on the shape of the features and wind direction. Discrepancies between the number of oil slick polygons and OSO points are due to some oil slicks being represented as segments of discrete seepage events (i.e., multiple polygons).

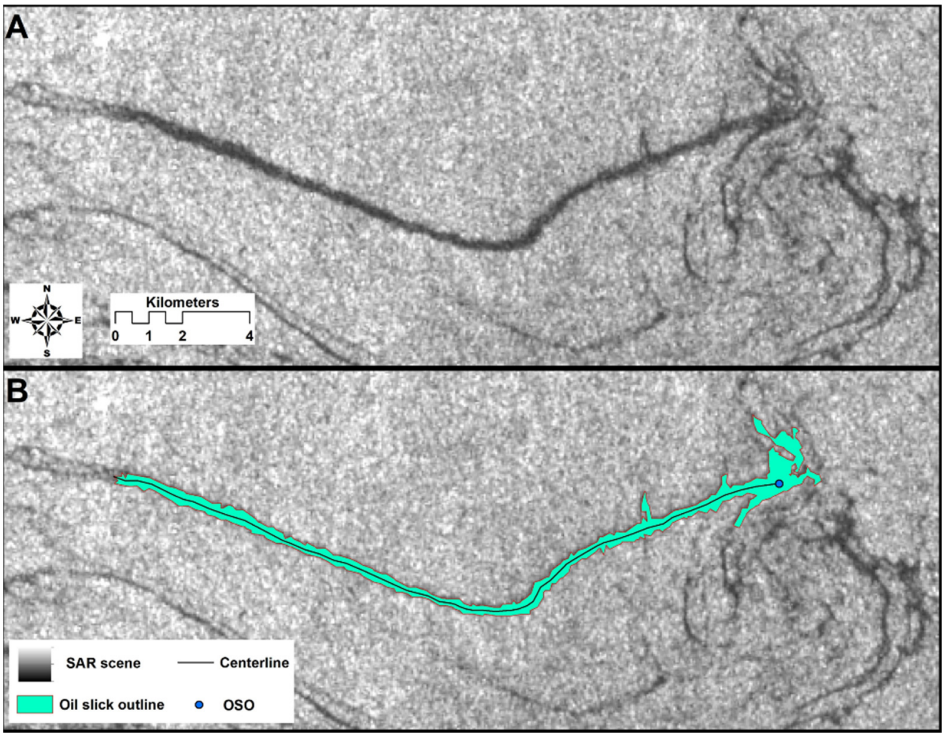

Figure 2. (**A**) Example SAR image with oil slick and (**B**) SAR image with natural oil slick polygon, centerline, and OSO.

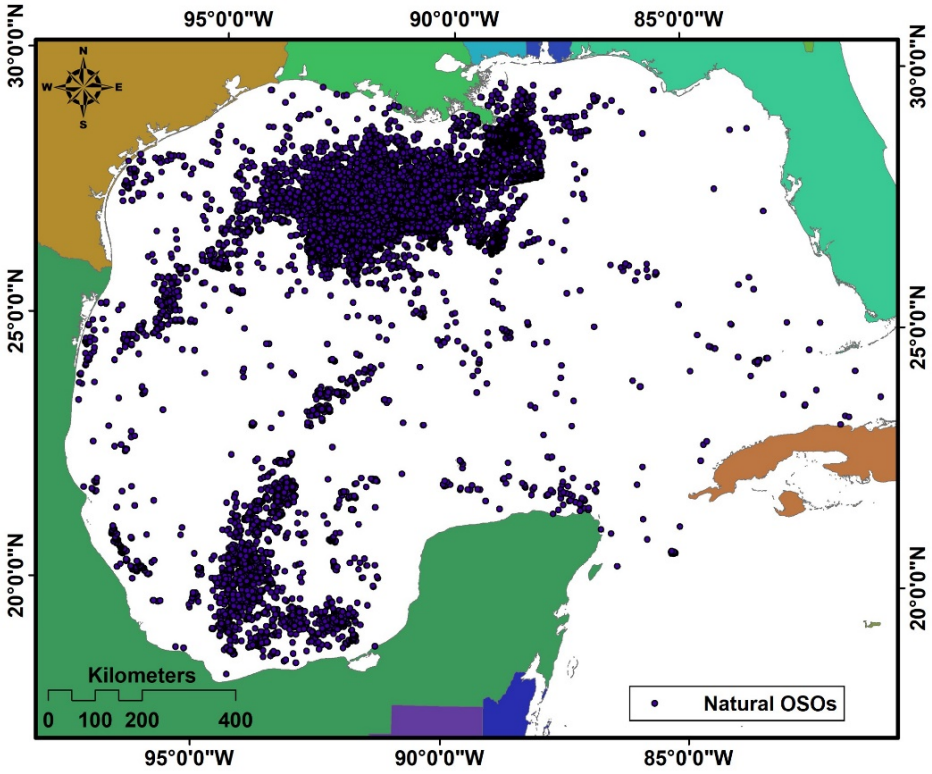

Figure 3. Locations of interpreted natural OSOs in the Gulf of Mexico.

2.2. Defining Seep Zones

The point aggregation method in ArcMap is used to define seep zones in the Gulf of Mexico. This method creates polygons with a minimum of three points, forming a cluster within a set aggregation distance [73]. A shapefile consisting of all points categorized as natural seepage OSOs was the input feature, and the aggregation distance was set to 1000 m. Seep zones are typically within an area of 1000 m × 1000 m and contain one to several interconnected vents [7,67,74]. Due to variability at the surface from currents, 1000 m is the most conservative estimate of the distance between OSOs that belong to the same seep zone. Although OSOs originating from a particular seep zone may have been excluded, the 1000 m aggregation distance likely captures the centroid of the seep zone and the OSOs that are most representative of the vents supplying the seep zone. Following point aggregation, centroids of the polygons were extracted and converted to points to define the center of the seep zones. Seep zones were subsequently analyzed for flux, recurrence rate, and associated geologic features.

2.3. Centerline Flux Estimation

Oil slicks from seeps are typically broadest at the OSO, where oil is continually surfacing, then dissipate as the oil ages along a curvilinear drift path and degrade terminally to traces that can no longer be detected by SAR (Figure 2). The length of the centerline of each slick from its OSO to its termination reflects the drift path of the slick and therefore provides a basis for estimating the age of each slick (Meurer et al., in prep.). The "centerline" flux method calculates the distance that oil travels per unit time using a forcing magnitude calculated as 75% of the average wind and 100% of the average current speed for a specified region. The age of each slick (i.e., residence time) is determined by dividing the centerline length by the forcing magnitude. Flux is then estimated by converting the oil slick area to a volume, using an assumed oil thickness of 0.1 µm, and dividing the volume by slick age. This calculation provides the average instantaneous flux required to generate the observed slick given its age and area. The centerline method was applied to all seepage slicks to

generate flux estimates for individual slicks. The individual estimates were averaged to generate fluxes for seep zones.

3. Results

3.1. Seep Zones

The point aggregation method identified 1618 seep zones, containing 16,125 of the natural OSOs, in the Gulf of Mexico (Figure 4). Of the 1618 seep zones, 1401 were located in the northern Gulf of Mexico, in U.S. waters delineated by Bureau of Ocean Energy Management (BOEM) lease blocks. The majority of seep zones in the northern Gulf of Mexico are in the Louann salt formation and Sigsbee escarpment; a second seep zone aggregation was observed in the southern Gulf of Mexico over the Campeche knolls. The individual slicks originating within, but not wholly confined to, a given zone, are snapshots of discharge rates from that zone, capturing the combination of the flux of oil to the surface and its residence time before the oil dissipates under synoptic oceanic conditions and is no longer visible to SAR.

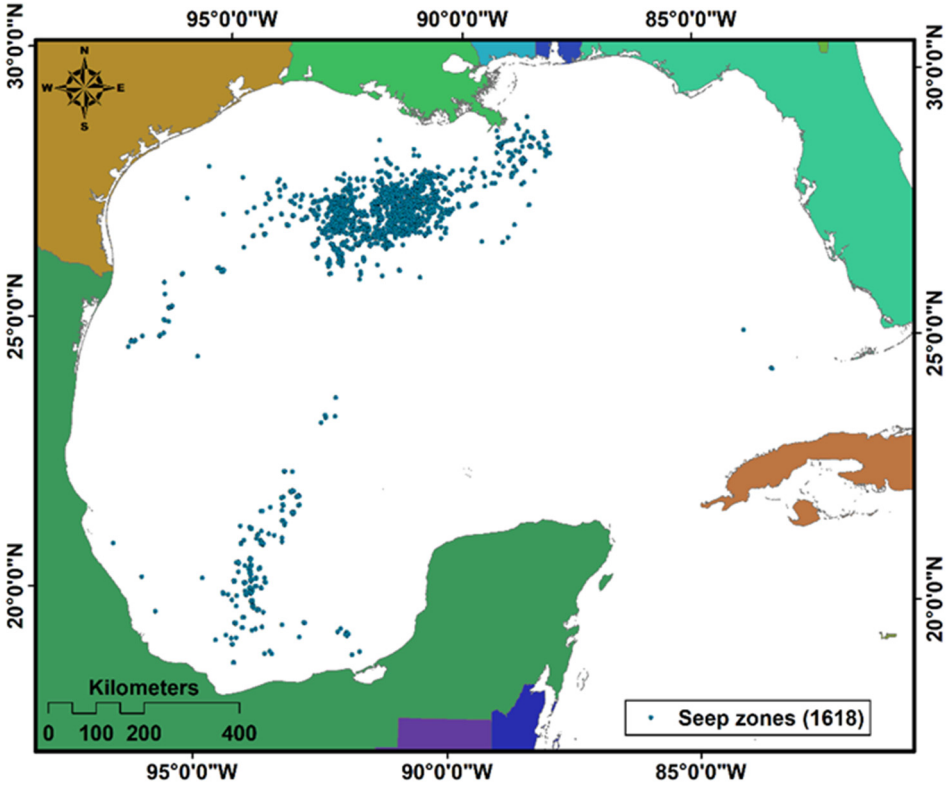

Figure 4. Centroids of seep zones identified using point aggregation.

3.2. Flux Estimates

The temporal variability of flux in the Gulf of Mexico was analyzed using a sequence of flux estimates for all OSOs, excluding years with fewer than 50 total scenes. The average flux of natural oil in the Gulf of Mexico was consistently higher from 1992 to 1995, with no discernible trend between 1995 and 2017, when data were normalized by the number of scenes containing oil slicks (Figure 5A). Normalizing data by the area of scenes containing oil slicks suggests a decrease in flux after 1995 (Figure 5B). However, there is a bias in the coverage of SAR scenes from 1992 to 1995, where highly productive areas were targeted. To control for area and scene bias, we examined the temporal variability of flux in four lease blocks extending from the western Gulf of Mexico (AC857), through the most productive region (GB647 and GC600), to the eastern edge of the most productive region (MC709). The average flux of oil in the four lease blocks fluctuates, but there is no discernible increase or decrease over time (Figure 6A). The zonal variability of oil seepage was examined by

choosing lease blocks located in the most productive region of the Gulf of Mexico, exhibiting similar recurrence rates, but variable average flux rates. Lease blocks AC857 and GB647 exhibit significantly different fluxes (low and high, respectively); lease block AC857 also exhibits significantly low recurrence (Figure 6B).

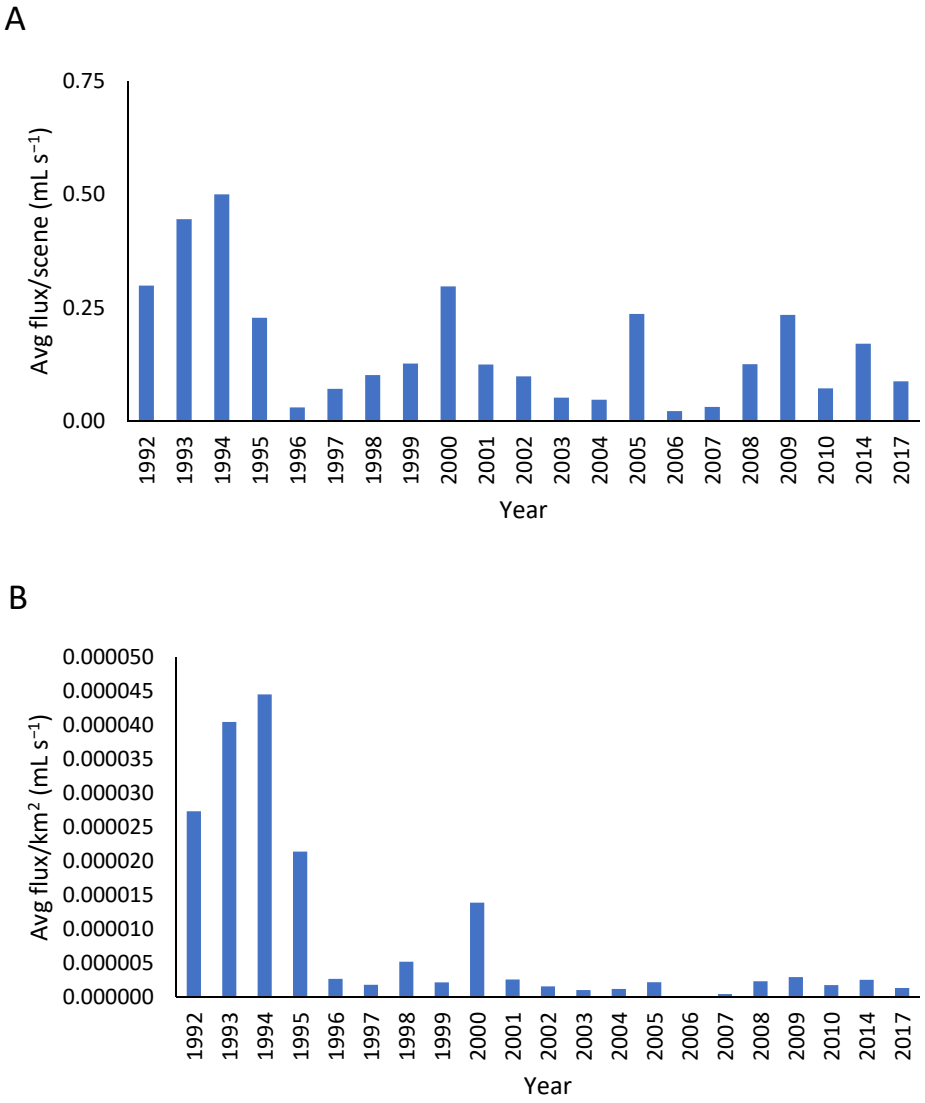

Figure 5. Temporal variation of average flux of natural OSOs in the Gulf of Mexico. (**A**) Average flux is normalized by the number of scenes containing oil slicks per year. (**B**) Average flux is normalized by the area of scenes containing oil slicks per year. Years with <50 total scenes were excluded for this analysis.

Flux estimates for individual OSOs were used to calculate the average flux for each seep zone. The average flux for natural oil seeps in the Gulf of Mexico, as represented by SAR imageable slicks, is approximately 9.8 mL s^{-1} (1.9×10^3 bbl yr^{-1}). However, using the average flux of seep zones assumes a constant rate, despite the existence of known episodic and ephemeral seeps. To estimate the flux of seep zones over longer times, the average flux is weighted by the recurrence rates of slicks for each seep zone. The recurrence rate of each seep zone was calculated by dividing the number of scenes where oil slicks were observed by the total number of scenes captured over that seep zone (only weather-compliant scenes are included in this study). The recurrence rate is the ratio of the number of times a slick is observed for a seep zone and the number of times that seep zone was examined; the average recurrence rate is 11%. The frequency distribution of seep zone recurrence is skewed to the right, with an asymmetry in the low side distribution (Figure 7). The average

flux for each seep zone was multiplied by the recurrence rate; the flux range was calculated as the weighted average flux of all seep zones ± one standard deviation (SD). The flux of natural oil seep zones, incorporating the recurrence rate of each seep zone, ranges from 1.73 - 6.69 × 10^5 bbl yr^{-1} (2.75–10.63 × 10^4 m^3 yr^{-1}). There is a weak positive correlation, but no relationship between the average flux of seep zones and recurrence rate (Figure 8).

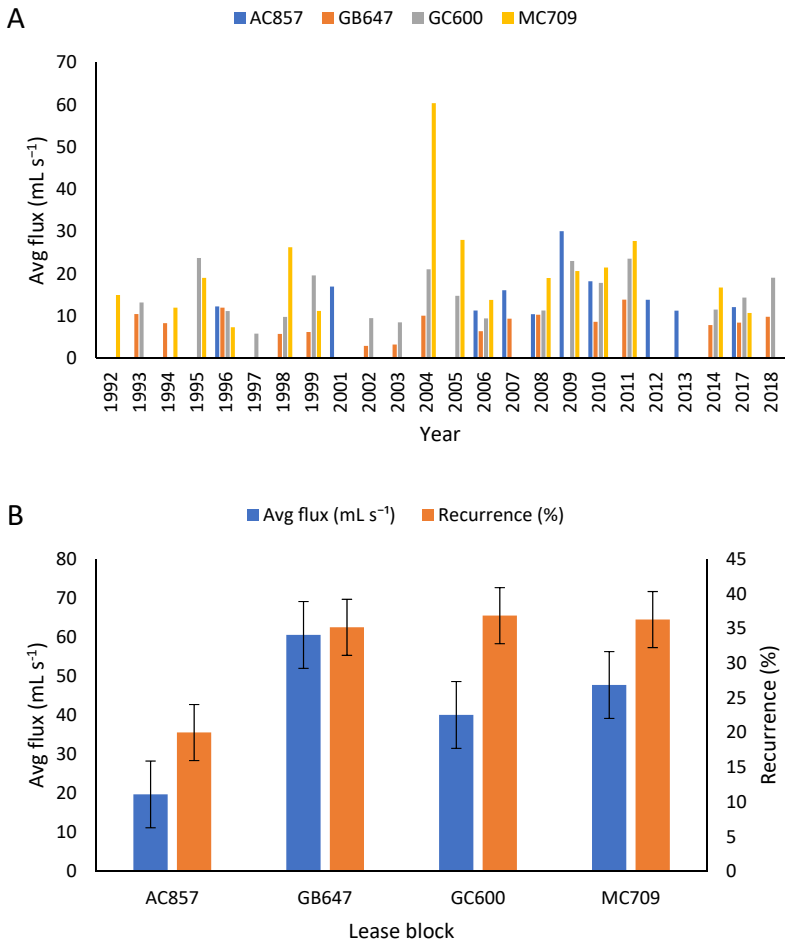

Figure 6. (**A**) Temporal variability of average flux in lease blocks extending from west (AC857) to east (MC709) across the Gulf of Mexico. (**B**) Zonal variation of average flux and recurrence rates in lease blocks. Error bars represent standard error.

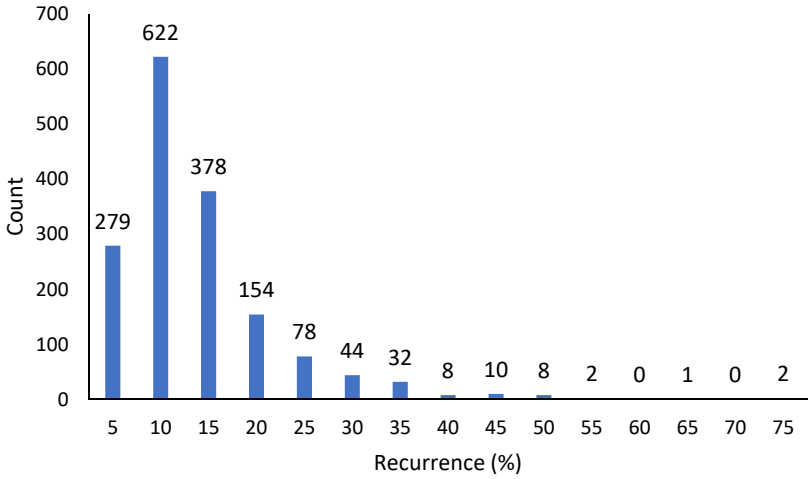

Figure 7. Frequency distribution of seep zone recurrence rates.

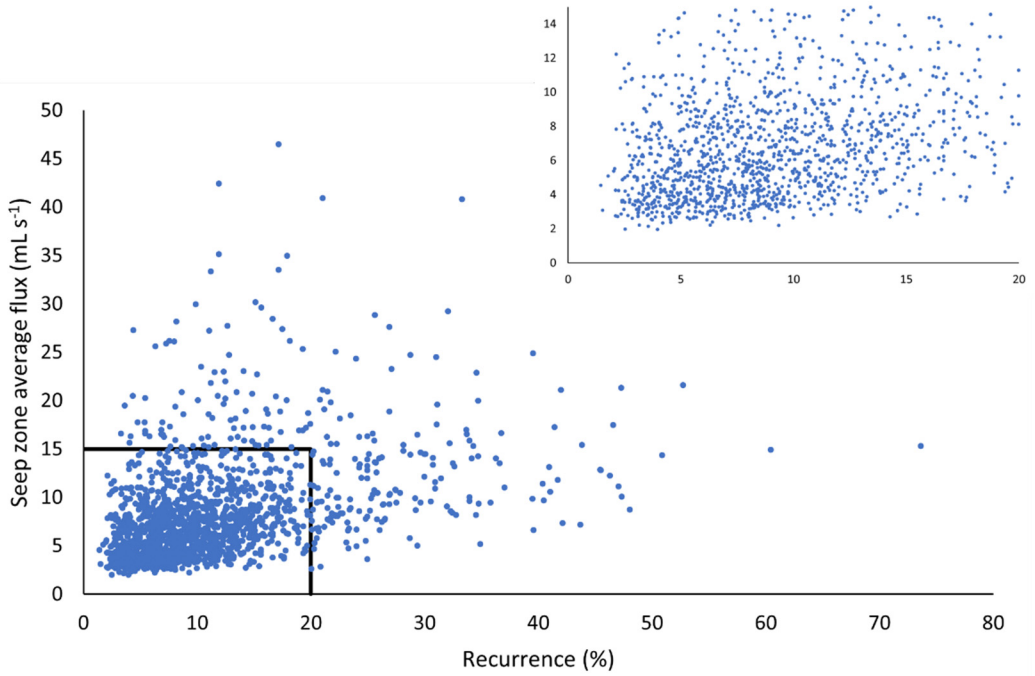

Figure 8. Comparison of recurrence rate and average flux of seep zones. Inset enlarged to show lack of relationship or correlation between recurrence rate and average flux.

The total estimated flux of oil in the Gulf of Mexico was derived from average flux estimates of discrete seep zones. The frequency distribution of seep zone average flux is skewed to the right (Figure 9). Seep zone average flux was then compared to the depth of seep zones. There is bimodal behavior, where seep zones below ~2000 m exhibit higher average fluxes, but there is no relationship between the depth of a seep zone and average flux (Figure 10). The frequency distribution of the annual flux of each seep zone was plotted to understand how the flux of natural oil in the Gulf of Mexico is distributed among seep zones. It is strongly skewed to the left. Of the 1618 discrete seep zones, 167 discharge greater than 500 bbl yr^{-1} (Figure 11).

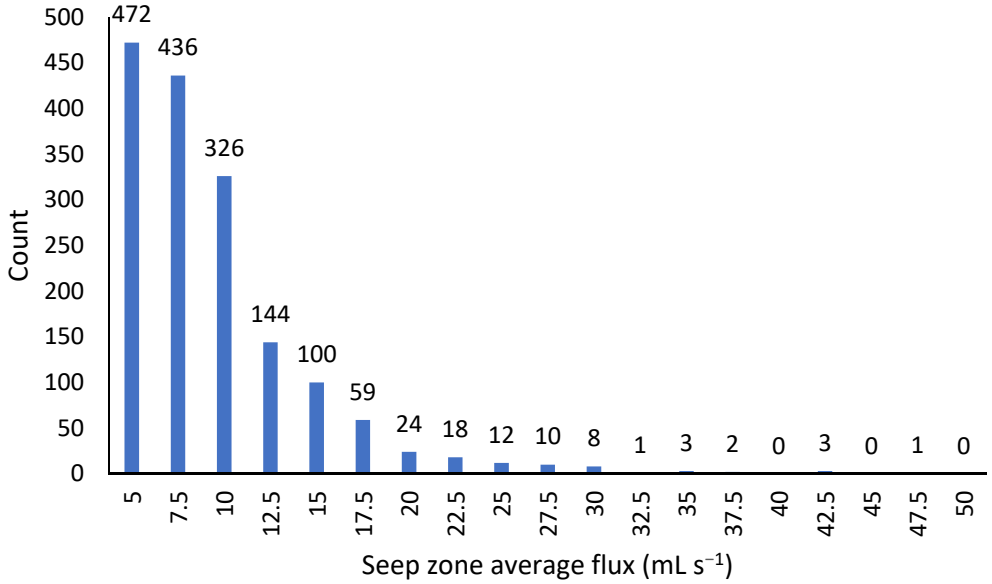

Figure 9. Frequency distribution of average flux of seep zones.

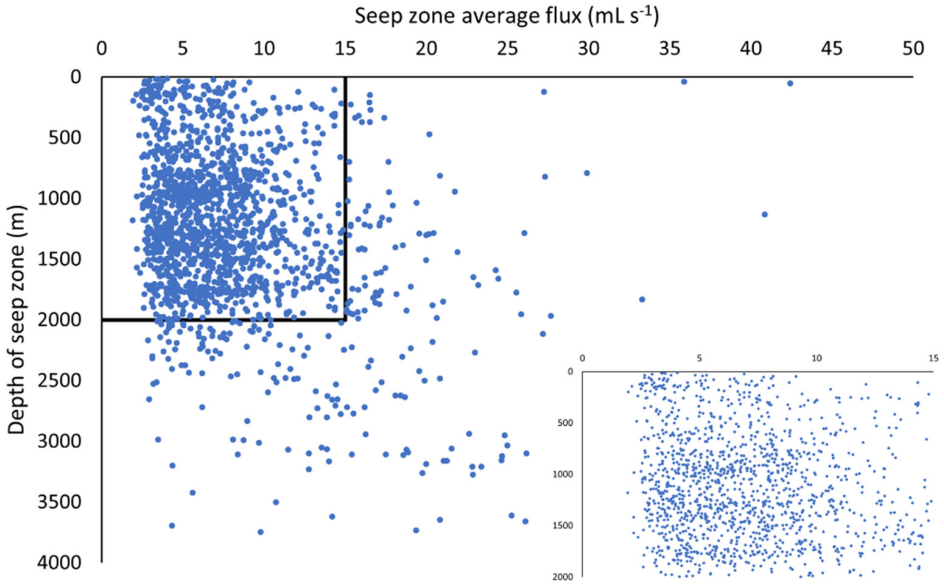

Figure 10. Comparison of seep zone depth to seep zone average flux. Inset enlarged to show lack of relationship between depth and average flux of seep zones.

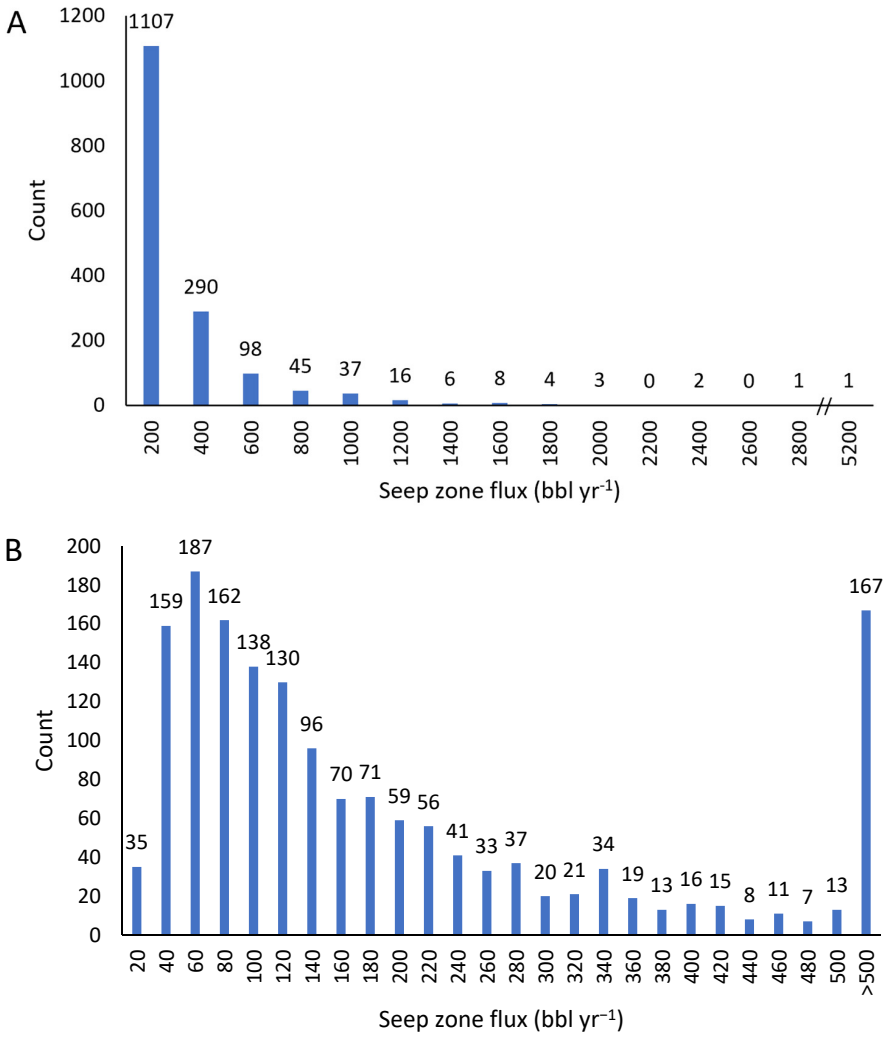

Figure 11. (**A**) Frequency distribution of seep zone annual flux. (**B**) Frequency distribution of seep zone annual flux for the majority of seep zones.

3.3. Seep Zone Categories

Seep zones were categorized by flux and recurrence rates to determine which seep zones discharge the most oil and are active most frequently. Means and SD for flux and recurrence were calculated and seep zones with rates 2 SD $\geq$ mean rates were considered significantly different. Of the 1401 identified seep zones in U.S. waters, a subset of 70 were identified as exhibiting the highest flux and recurrence rates: 16 exhibit high flux, 52 exhibit high recurrence, and 2 exhibit both high flux and high recurrence rates (i.e., the most prolific seep zones). High flux seep zones discharge oil at rates of $\geq$18.51 mL s^{-1} and high-recurrence seep zones are active at rates of $\geq$27.57% (Figure 12). These seep zones are located in the most productive region of the Gulf of Mexico (Figure 13). The subset of seep zones was then analyzed for associations with geologic features identified by BOEM; approximately 37,000 seismic anomalies were identified in the northern Gulf of Mexico that exhibit high (positive) or low (negative) acoustic amplitudes compared to background levels [75]. With the use of ArcMap tools, BOEM defined anomalies were spatially joined to seep zones if they were within a 1000 m radius of the seep zone. Although the 1000 m radius was used to define seep zones, it is not sufficient to capture all associated seafloor geologic features, especially in deeper waters, due to deflection by subsurface currents. Approximately half of the prolific seep zones in U.S. waters were not associated with anomalies via the spatial join process; these seep zones were examined manually using the BOEM bathymetry data [76] from which the anomalies were originally derived. Approximately 97% of the prolific seep zones were found to be associated with seismic anomalies: 50/52 high recurrence, 16/16 high flux, and 2/2 high recurrence and flux. All seep zone categories were more likely to be associated with positive anomalies. However, there was not a significant relationship between seep zone category and association with seismic anomalies (X^2 (2, n = 140) = 0.13, $p > 0.05$; Table 3).

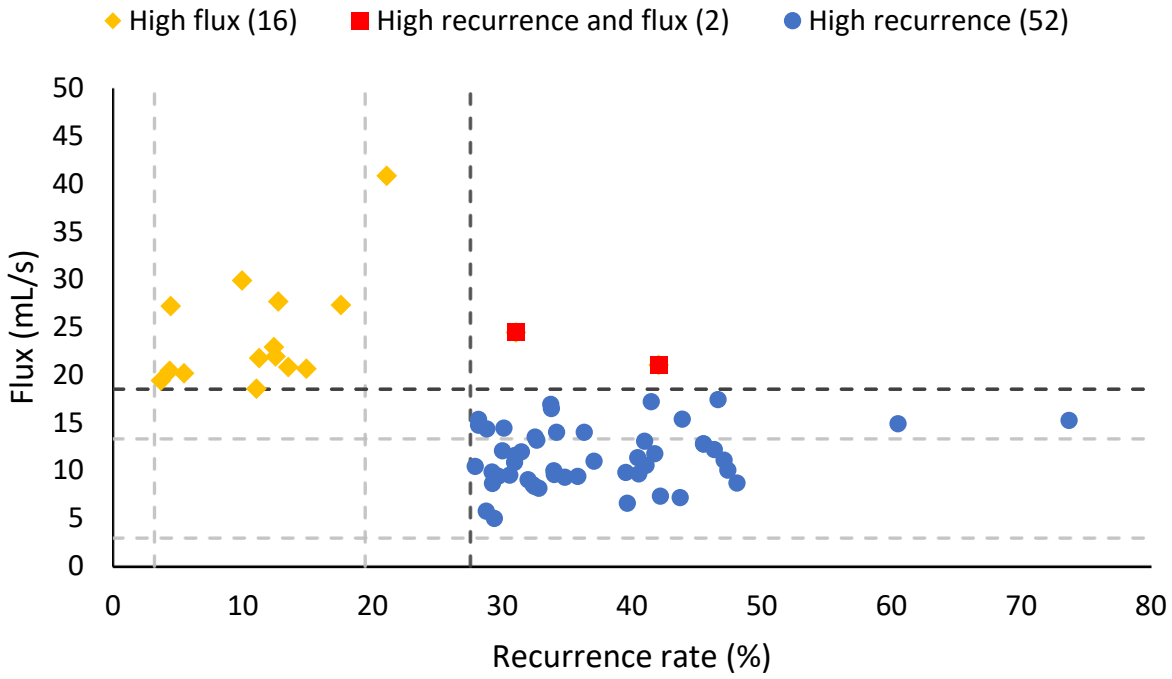

Figure 12. Distribution of seep flux and recurrence rates exhibited by the subset of more oily and more active seep zones. The light gray dashed lines indicate rates that are ±1 SD and the dark gray dashed lines indicate rates that are +2 SD.

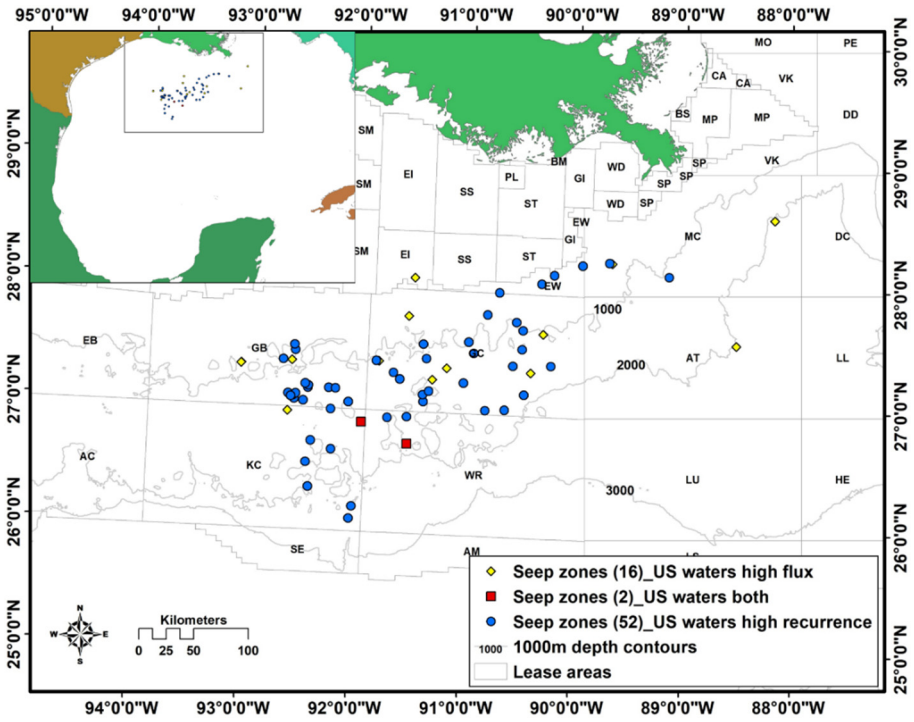

Figure 13. Locations of seep zones exhibiting rates of high flux, high recurrence, and both high flux and recurrence (i.e., 2 SD $\geq$ mean rate).

Table 3. Number of categorized seep zones associated with positive and negative BOEM seismic anomalies. Note that an individual seep zone may be associated with multiple positive and/or negative anomalies, resulting in totals greater than the number of prolific seep zones.

Seep Zone Category	Positive Anomaly	Negative Anomaly	Total
High recurrence	72	28	100
High flux	27	9	36
High recurrence and high flux	3	1	4
Total	102	38	140

4. Discussion

Remote sensing techniques, specifically SAR, have been used extensively to detect oil slicks on the ocean surface around the world [3,4]. However, delineating seep zones, estimating flux, and identifying relationships between seep zones and geologic features remains challenging. By compiling all oil slicks classified as natural seepage by the vendors and MacDonald et al. [11], we evaluated the spatial distribution of OSOs to define discrete seep zones. With an understanding of OSO distribution, we calculated the flux and recurrence rate of the seep zones to estimate the annual natural seepage of oil in the Gulf of Mexico. Given a useful technique for estimating the flux and recurrence rate of seep zones, we can consider how to improve the knowledge of the seepage in the Gulf of Mexico, as well as provide a model for a more global understanding of natural oil seepage.

The greater SAR surveillance coverage of the Gulf of Mexico available for this study allowed a more focused spatial analysis of OSOs and their seafloor sources (i.e., seep zones). The OSOs of natural oil slicks located in regions with persistent seepage, as captured by repeated SAR imagery, can be clustered into discrete seep zones. The 1618 identified seep zones represent clustered vents connected to the same hydrocarbon migration system. The quantity of identified seep zones is not equal to the number of discrete vents on the seafloor. Seep zones represent the area containing one to many vents that are generating oil slicks observed within a geographic area. Previous seep zone studies estimated a 3500 m maximum deflection radius for oil, between the seafloor source and surface detection;

deflection is dependent on water depth [7]. The point aggregation technique used in this study did not incorporate water depth as a parameter capable of influencing the deflection of oil, which influences the number of OSOs associated with a seep zone. The OSOs may have been deflected out of the 1000 m aggregation distance used to delineate the seep zones. OSOs that were potentially deflected into a seep zone from which they did not originate were not included in the quantification of seep zones. Due to the large number of OSOs and OSO density in our dataset, using the 3500 m radius [7] would have resulted in fewer seep zones than identified in MacDonald et al. [11] by including OSOs deflected into a seep zone from an adjacent seafloor source. Some of the OSOs that were not included in our seep zones likely belong to the same hydrocarbon systems that supply the seep zones. Identifying fewer seep zones would likely result in a higher recurrence rate because each seep zone would contain more slicks. However, the basin-scale flux is unlikely to change substantially with the number of seep zones since the seep zone centroids identified in this study represent the areas in the Gulf of Mexico with the most oil discharge. It is likely that there are more seep zones in the Gulf of Mexico that we did not identify due to the point aggregation parameter requiring a minimum of three OSOs to form a seep zone. However, the seep zones are representative of the location and flux of the most influential seepage areas.

Previous studies of oil and gas fluxes from seeps focused on short-term, on-bottom time series analyses [5,77], while the large-scale SAR surveillance system utilized by the present study provided a unique opportunity to examine basin-scale natural oil seepage over time and space. The average flux of natural oil in the Gulf of Mexico appears to have decreased after 1995 (Figure 5). Research has shown evidence for decreased seepage in the Coal Oil Point hydrocarbon system related to associated oil and gas production [78,79]. However, the Gulf of Mexico flux estimates relied on lower-resolution imagery and bias in scene coverage, which may have influenced the size of slicks captured by SAR, and the average flux in a given year. Normalizing the average flux of OSOs by the number of scenes containing slicks per year (Figure 5A) accounts for temporal variation in scene coverage. The fewest number of scenes containing oil slicks were captured in 1993 (16/59) and the highest number of scenes containing oil slicks in 1996 (302/681). However, normalizing for the number of scenes containing oil slicks does not account for the areal coverage of the scenes (Figure 5B). Considering the area of the Gulf of Mexico that contains natural oil seepage each year is more representative of the nature of the underlying hydrocarbon system. Additionally, the scene area in the early 1990s was generally smaller than the area in later years, while the average flux was similar across all years, resulting in the higher fluxes observed in Figure 5B. This bias may exaggerate the perceived decrease in average flux after 1995. Normalizing the Gulf of Mexico data by both the number of scenes with slicks and by the area covered by scenes with slicks begins to correct for discrepancies in scene size and resolution. Although both methods of data normalization exhibit consistently higher average flux between 1992 and 1995, followed by a decrease and stabilization, additional study is required to determine if average flux has decreased over time due to production activities. Artifacts in the SAR data and the natural variability of seep zones (i.e., less seeps were active in recent years) must also be considered. However, the temporal variation of average flux in four lease blocks across the Gulf of Mexico (Figure 6) indicates that production does not affect the natural hydrocarbon system on a human timescale. Approximately 18.3 billion bbl of crude oil were produced between 1981 and 2021 [80] and production activities are expected to increase by the end of 2022 [10]. SAR surveillance of the new projects and the collection of more SAR scenes with higher resolutions may begin to resolve these issues and further constrain flux estimates.

Without direct seafloor visual measurements, analysis of slicks provides the most robust method of estimating oil flux. The residence time for oil slicks detected by remote sensing is the period during which oil reaching the surface will continue to dampen capillary waves to make a visible slick. MacDonald et al. [11] proposed this critical variable to be 8–24 h. Subsequent modeling of ocean conditions and oil slick appearance in the Gulf

of Mexico yielded a mean residence time of 6.4 h [58]. A shorter residence time implies a higher flux rate to produce a given oil slick. The centerline method calculates oil slick ages using the centerline length of each slick and dividing by the average forcing magnitude, so the unique residence time is calculated for each slick. Oil slick age, as estimated by the centerline method, is necessary for quantifying seep discharge [69].

The present study agrees reasonably with the previous annual flux estimates of MacDonald et al. [11] despite using different methodologies. Both studies assumed a 0.1 µm oil slick thickness to convert areas to volumes, but the present study estimated an individual residence time for oil slicks, with an average of 6.3 h (agreeing more closely with [69]), instead of assuming a residence time of 8–24 h. The residence time calculation in MacDonald et al. [11] corresponds to the amount of time required to accumulate the oil seen in the SAR scenes; an 8 h residence time corresponds to three times as much oil seepage as a 24 h residence time. Based on our estimated residence time of 6.3 h, the higher end of the flux range estimated by MacDonald et al. [11] is likely ~ 20% too low. The present study also considered the recurrence rates of seep zones, which were not considered by MacDonald et al. [11], because individual vents have differing timescales of activity [67,69]. Although seep zones exhibited an 11% recurrence rate, on average, the flux estimate still closely agreed with the previous flux estimates for the Gulf of Mexico. MacDonald et al. [11] generated an average slick distribution using a bootstrap resampling of all of their data; this should compensate for the recurrence rate variability if the sample set is large enough. The close match between the two estimations suggests that the underlying assumptions used in the different flux estimation methodologies and the amount of observations each included are adequate to describe the surface expression of hydrocarbon systems in the Gulf of Mexico.

The Gulf of Mexico results demonstrate a high degree of temporal variability in seep zones. Among the 1618 seep zones delineated in the present study, the average recurrence rate of 11% is the result of combined geologic processes and ocean conditions that limit formation of surface oil slicks. The seep zone recurrence rates included some highly active seep zones (70%), as might be expected given the regional character of the Gulf of Mexico; however, the majority of seeps were active in fewer than 14% of observations. The frequency distribution of seep zone recurrence rates (Figure 7) exhibits an asymmetry in the low side distribution. Low recurrence seep zones were necessarily excluded because they did not generate the minimum number of OSOs during the SAR surveillance period to create a seep zone. This observation may be influenced by current SAR technologies. Seep zones with higher flux rates are more likely to be captured by lower-resolution SAR scenes; as the resolution increases, seep zones with lower discharge will be observed more often. Recurrence rates from the Gulf of Mexico are comparable to those from similar hydrocarbon basins. Jatiault et al. [69] found a recurrence rate of approximately 15% among natural seeps of the Congo Basin, but few other studies have accessed sufficient SAR coverage to assess the variability in other regions. Although the recurrence rate is currently unknown in most productive ocean basins, the low average recurrence rates in both the Gulf of Mexico and the Congo Basin suggest that a large number of observations are required to reliably image the seepage from the significant majority of seeps in a basin. The variability of output from natural seeps argues against extrapolating flux from limited satellite scene coverage to a basin-scale estimate, especially given the relatively low number of prolific seep zones.

Our estimated flux of natural oil in the Gulf of Mexico can be compared to flux rates in other highly productive regions. Annually, Coal Oil Point releases 1.4–7.3 $\times$ 10^4 bbl y^{-1} of oil into the waters offshore Santa Barbara, CA [77], the Black Sea releases 2.8 $\times$ 10^4 bbl y^{-1} of oil [34], and the Congo Basin releases approximately 2.75 $\times$ 10^4 bbl y^{-1} [69]. The estimated 1.73–6.69 $\times$ 10^5 bbl yr^{-1} released in the Gulf of Mexico is an order of magnitude larger than other productive hydrocarbon basins, even those with similar underlying geology. Seep zones in the Gulf of Mexico discharging oil from greater depths may discharge oil at higher average rates; otherwise, the oil would be deflected out of its seep zone of origin, or the oil may not make it to the sea surface and be detected by SAR. The close

agreement between our estimate, which used a more comprehensive dataset, and that of MacDonald et al. [11] indicates that the natural seepage rate in the Gulf of Mexico is now reasonably well constrained. However, these estimates are derived from SAR imagery with pixel resolutions of 100–400 m. Satellites capable of 10 m resolution (e.g., Sentinel SAR) may yield smaller overall oil slick areas by resolving oil-free water within a given oil slick, reducing estimated fluxes. However, smaller slicks not detected by lower-resolution imagery will be detected, which may offset the potential decrease in slick area. The flux of seep zones, especially the significant seep zones, is unlikely to change substantially. We examined a subset of 70 seep zones that displayed the highest average oil fluxes and recurrence rates in our dataset, including 68 seep zones associated with primarily positive seismic anomalies defined by BOEM [75]. All 70 seep zones are located on domes and ridges (i.e., not in basins) generated by halokinesis, where diapirism created migration pathways for hydrocarbons from the source rock to the seafloor [8]. High-flux and high-recurrence seep zones were associated with geologic features such as mud volcanoes and pockmarks. Two of the lease blocks used to examine the temporal variability of flux (Figure 6) correspond to significant seep zones. Lease blocks GC600 and MC709 contain seep zones that exhibit high recurrence; MC709 is also adjacent to a high-flux seep zone (Figures 12 and 13). The analysis of temporal variability includes highly active seep zones, indicating that recurrence may remain stable over extended periods of time. However, including highly active (i.e., not average) seep zones may conceal evidence of a change in average flux over time. Note that this analysis was limited to the northern Gulf of Mexico, where seismic anomaly data are available; seeps from Mexican waters were not included. Additional study is required to understand the relationships between seismic anomalies and the flux and recurrence rate of seep zones.

SAR detection of oil slicks is limited by resolution and bias in areas targeted. The average recurrence rate of seep zones categorized as high flux was 14%, greater than the 11% average recurrence rate of all seep zones, but too low to be categorized as high recurrence. Our seep zone delineation methodology inherently discriminates against the lowest-recurrence seepage events because it requires a minimum of three OSOs and thereby sets a lower limit on the recurrence rate. As higher-resolution data become available, seepage events with lower fluxes will be captured. This will likely lead to an increase in the recurrence and identification of additional seep zones. However, assuming that additional slicks identified from a given seep zone have smaller fluxes, the increase in the recurrence rate will be offset by a lower average flux and will be unlikely to cause significant changes in estimates for annual flux in the Gulf of Mexico. The flux of oil naturally entering the marine system is not significant as an acute environmental threat, but may result in chronic impacts that are less easily recognized. The spatial and temporal distribution of oil in the Gulf of Mexico is important to hydrocarbon exploration, the regulation of offshore oil production platforms, and oil pollution monitoring [55–57,61]. Higher-resolution data will capture the presence of surface slicks in areas that were previously unidentified, indicating the potential for resource exploitation in the area. Additionally, seepage events exhibiting low flux and low recurrence will be captured; if these slicks are located near platforms, management will be able to identify the source as being natural or anthropogenic. Although our results may be influenced by the limitations of SAR imagery, our analysis likely accounted for all seepage events that have a large influence in the Gulf of Mexico basin.

5. Conclusions

This study provides a comprehensive view of natural oil seepage in the Gulf of Mexico, resolved in space and time on the scale of individual seepage events. The focus on, and quantification of, discrete events provides the opportunity for the investigation of seepage processes not possible by the analysis of oil coverage over entire satellite scenes. Natural seepage rates for the Gulf of Mexico estimated in the present study are in close agreement with earlier estimates. That the two different approaches produced similar estimates suggests that natural seepage rates for the Gulf of Mexico are now

reasonably well constrained. The identified seep zones provide a useful representation of the Gulf's hydrocarbon system by depicting areas of clustered slicks. Flux and recurrence rate calculations revealed a high degree of temporal variability among seep zones; however, there is no apparent relationship between seep zone average flux and recurrence rate. A relatively small number of statistically different seep zones with high flux, recurrence, or both were identified. These were found to be associated with seismic anomalies and seafloor geologic features identified by BOEM. Detailed comparison of seep zone locations and seafloor features has the potential to yield insights into the nature of natural hydrocarbon release processes, but is beyond the scope of this effort. In contrast to what is observed in the Santa Barbara Channel, temporal and zonal analysis of flux indicates that the extensive oil production activities in the Gulf of Mexico have not meaningfully impacted natural seepage.

The methods developed through the first application of a basin-scale SAR surveillance system for this study could be applied on a global scale. As the archive of SAR imagery from the Sentinel platforms increases and adds to the existing data, much of the continental shelf and slope can be studied for evidence of natural oil seepage. Using similar datasets, the global magnitude of natural seepage can be assessed, with implications for seep communities, understanding processes related to oil migration, and potential resource exploitation. A similar approach could be used to study pollution slicks generated from subsea sources and for monitoring sites of persistent pollution.

Author Contributions: Conceptualization, C.O., W.P.M. and I.R.M.; methodology, C.O., M.S., S.D.A., W.P.M. and I.R.M.; data curation, C.O.; writing—original draft preparation, C.O.; writing—review and editing, M.S., S.D.A., W.P.M. and I.R.M.; funding acquisition, W.P.M. and I.R.M. All authors have read and agreed to the published version of the manuscript.

Funding: This work was funded, in part, by a grant (2018FSU1) from ExxonMobil Upstream Research Company to Ian MacDonald and Florida State University. W.P.M. thanks ExxonMobil Upstream Research Company for their support of this work and for agreeing to release the findings.

Conflicts of Interest: W.P.M was employed by ExxonMobil Upstream Research Company during the period this research was conducted. The findings of this research have no bearing on any financial or public relation concerns of ExxonMobil Corporation.

References

1. Kennicutt, M.C.; Brooks, J.M.; Denoux, G.J. Leakage of deep, reservoired petroleum to the near surface on the Gulf of Mexico continental slope. *Mar. Chem.* **1988**, *24*, 39–59. [CrossRef]
2. Abrams, M.A. Geophysical and geochemical evidence for subsurface hydrocarbon leakage in the Bering Sea, Alaska. *Mar. Pet. Geol.* **1992**, *9*, 208–221. [CrossRef]
3. Kvenvolden, K.A.; Cooper, C.K. Natural seepage of crude oil into the marine environment. *Geo-Mar. Lett.* **2003**, *23*, 140–146. [CrossRef]
4. Ivanov, A.Y.; Gerivani, H.; Evtushenko, N.V. Characterization of natural hydrocarbon seepage in the South Caspian Sea off Iran using satellite SAR and geological data. *Mar. Georesour. Geotechnol.* **2020**, *38*, 527–538. [CrossRef]
5. Johansen, C.; Todd, A.C.; MacDonald, I.R. Time series video analysis of bubble release processes at natural hydrocarbon seeps in the Northern Gulf of Mexico. *Mar. Pet. Geol.* **2017**, *82*, 21–34. [CrossRef]
6. MacDonald, I.R.; Guinasso Jr., N.L.; Ackleson, S.G.; Amos, J.F.; Duckworth, R.; Sassen, R.; Brooks, J.M. Natural Oil Slicks in the Gulf of Mexico Visible From Space. *J. Geophys. Res.* **1993**, *98*, 351–364.
7. Garcia-Pineda, O.; MacDonald, I.; Zimmer, B.; Shedd, B.; Roberts, H. Remote-sensing evaluation of geophysical anomaly sites in the outer continental slope, northern Gulf of Mexico. *Deep-Sea Res. II* **2010**, *57*, 1859–1869. [CrossRef]
8. Kennicutt, M.C., II. Oil and Gas Seeps in the Gulf of Mexico. In *Habitats and Biota of the Gulf of Mexico: Before the Deepwater Horizon Oil Spill*; Ward, C.H., Ed.; SpringerOpen: New York, NY, USA, 2017; pp. 275–358.
9. MacDonald, I.R.; Sager, W.W.; Peccini, M.B. Gas hydrate and chemosynthetic biota in mounded bathymetry at mid-slope hydrocarbon seeps: Northern Gulf of Mexico. *Mar. Geol.* **2003**, *198*, 133–158. [CrossRef]
10. U.S. EIA. Gulf of Mexico Crude Oil Production will Increase with New Projects in 2021 and 2022. Available online: https://www.eia.gov/todayinenergy/detail.php?id=47536#:~{}:text=In%202020%2C%20GOM%20crude%20oil,at%201.9%20million%20b%2Fd (accessed on 2 May 2022).
11. MacDonald, I.R.; Garcia-Pineda, O.; Beet, A.; Daneshgar Asl, S.; Feng, L.; Graettinger, G.; French-McCay, D.; Holmes, J.; Hu, C.; Huffer, F.; et al. Natural and unnatural oil slicks in the Gulf of Mexico. *J. Geophys. Res. Ocean.* **2015**, *120*, 8364–8380. [CrossRef]

12. Agirrezabala, L.M.; López-Horgue, M.A. Environmental and ammonoid faunal changes related to Albian Bay of Biscay opening: Insights from the northern margin of the Basque-Cantabrian Basin. *J. Sea Res.* **2017**, *130*, 36–48. [CrossRef]
13. Barberes, G.A.; Spigolon, A.L.D.; Pena dos Reis, R.; Permanyer, A.; Barata, M.T. Hydrocarbon seeps from the unconventional petroleum system of the South Portuguese Zone, Portugal. *J. Iber. Geol.* **2020**, *46*, 1–19. [CrossRef]
14. Bernardo, L.M.; Bartolini, C. Petroleum source rock analysis in the Western Caribbean Region: An overview. In *Petroleum Geology and Potential of the Colombian Caribbean Margin*; Bartolini, C., Mann, P., Eds.; AAPG Memoir 108; American Association of Petroleum Geologists: Tulsa, OK, USA; Repsol: Madrid, Spain; Anadarko: The Woodlands, TX, USA, 2015; pp. 587–614.
15. Bojesen-Koefoed, J.; Nytoft, H.P.; Christiansen, F.G. Age of oils in West Greenland: Was there a Mesozoic seaway between Greenland and Canada? *Geol. Surv. Den. Greenl. Bull.* **2004**, *4*, 49–52. [CrossRef]
16. Burns, K.A.; Brinkman, D.L.; Brunskill, G.J.; Logan, G.A.; Volk, H.; Wasmund, K.; Zagorskis, I. Fluxes and fate of petroleum hydrocarbons in the Timor Sea ecosystem with special reference to active natural hydrocarbon seepage. *Mar. Chem.* **2010**, *118*, 140–155. [CrossRef]
17. Camplin, D.J.; Hall, R. Neogene history of Bone Gulf, Sulawesi, Indonesia. *Mar. Pet. Geol.* **2014**, *57*, 88–108. [CrossRef]
18. Cazzini, F.; Dal Zotto, O.; Fantoni, R.; Ghielmi, M.; Ronchi, P.; Scotti, P. Oil and gas in the Adriatic Foreland, Italy. *J. Pet. Geol.* **2015**, *38*, 255–279. [CrossRef]
19. Chen, S.; Hu, C. In search of oil seeps in the Cariaco Basin using MODIS and MERIS medium-resolution data. *Remote Sens. Lett.* **2014**, *5*, 442–450. [CrossRef]
20. Coughlan, M.; Roy, S.; O'Sullivan, C.; Clements, A.; O'Toole, R.; Plets, R. Geological settings and controls of fluid migration and associated seafloor seepage features in the north Irish Sea. *Mar. Pet. Geol.* **2021**, *123*, 104762. [CrossRef]
21. Cramer, B.; Franke, D. Indications for an active petroleum system in the Laptev Sea, NE Siberia. *J. Pet. Geol.* **2005**, *28*, 369–384. [CrossRef]
22. Dill, H.G.; Kaufhold, S. The Totumo mud volcano and its near-shore marine sedimentological setting (North Colombia)—From sedimentary volcanism to epithermal mineralization. *Sediment. Geol.* **2018**, *366*, 14–31. [CrossRef]
23. Dupré, S.; Scalabrin, C.; Grall, C.; Augustin, J.-M.; Henry, P.; Celal Sengör, A.M.; Görür, N.; Çagatay, M.N.; Géli, L. Tectonic and sedimentary controls on widespread gas emissions in the Sea of Marmara: Results from systematic, shipborne multibeam echo sounder water column imaging. *J. Geophys. Res. Solid Earth* **2015**, *120*, 2891–2912. [CrossRef]
24. Feng, D.; Qiu, J.-W.; Hu, Y.; Peckmann, J.; Guan, H.; Tong, H.; Chen, C.; Chen, J.; Gong, S.; Li, N.; et al. Cold seep systems in the South China Sea: An overview. *J. Asian Earth Sci.* **2018**, *168*, 3–16. [CrossRef]
25. Fildani, A.; Hanson, A.D.; Chen, Z.; Moldowan, J.M.; Graham, S.A.; Arriola, P.R. Geochemical characteristics of oil and source rocks and implications for petroleum systems, Talara Basin, northwest Peru. *AAPG Bull.* **2005**, *89*, 1519–1545. [CrossRef]
26. Foster, K.L.; Stern, G.A.; Carrie, J.; Bailey, J.N.L.; Outridge, P.M.; Sanei, H.; Macdonald, R.W. Spatial, temporal, and source variations of hydrocarbons in marine sediments from Baffin Bay, Eastern Canadian Arctic. *Sci. Total Environ.* **2015**, *506–507*, 430–443. [CrossRef] [PubMed]
27. Freire, A.F.M.; Matsumoto, R.; Santos, L.A. Structural-stratigraphic control on the Umitaka Spur gas hydrates of Joetsu Basin in the eastern margin of Japan Sea. *Mar. Pet. Geol.* **2011**, *28*, 1967–1978. [CrossRef]
28. Freire, A.F.M.; Iemini, J.A.; Viana, A.R.; Magnavita, L.P.; Dehler, N.M.; Kowsmann, R.O.; Miller, D.J.; Bezerra, S.H.D.G.; dos Anjos Zerfass, G.d.S.; Shimabukuro, S.; et al. A giant oil seep at a salt-induced escarpment of the São Paulo Plateau, Espírito Santo Basin, off Brazil: Host rock characteristics and geochemistry. *Deep-Sea Res. Part II* **2017**, *146*, 45–52. [CrossRef]
29. Gbadebo, A.M. Environmental implications of bitumen seep induced pollution in parts of Ogun state, southwestern Nigeria. *Environ. Earth Sci.* **2010**, *59*, 1507–1514. [CrossRef]
30. Hakimi, M.H.; Al-Matary, A.M.; Ahmed, A.F. Bulk geochemical characteristics and carbon isotope composition of oils from the Sayhut sub-basin in the Gulf of Aden with emphasis on organic matter input, age and maturity. *Egypt. J. Pet.* **2018**, *27*, 361–370. [CrossRef]
31. Himmler, T.; Freiwald, A.; Stollhofen, H.; Peckmann, J. Late Carboniferous hydrocarbon-seep carbonates from the glaciomarine Dwyka Group, southern Namibia. *Palaeoecology* **2008**, *257*, 185–197. [CrossRef]
32. Hovland, M.; Jensen, S.; Fichler, C. Methane and minor oil macro-seep systems—Their complexity and environmental significance. *Mar. Geol.* **2012**, *332–334*, 163–173. [CrossRef]
33. Intawong, A.; Hodgson, N.; Rodriguez, K.; Hargreaves, P. Oil prospects in the Mozambique Channel: Where incipient subduction meets passive margin. *First Break* **2019**, *37*, 75–81. [CrossRef]
34. Ivanov, A.Y.; Matrosova, E.R.; Kucheiko, A.Y.; Filimonova, N.A.; Evtushenko, N.V.; Terleeva, N.V.; Libina, N.V. Search and Detection of Natural Oil Seeps in the Seas Surrounding the Russian Federation Using Spaseborne SAR Imagery. *Atmos. Ocean. Phys.* **2020**, *56*, 43–62. [CrossRef]
35. Ivanov, A.Y.; Gerivani, H. Oil leaking and seeping site in the Persian Gulf detected and studied by satellite observations. *Mar. Georesour. Geotechnol.* **2021**, *39*, 1481–1496. [CrossRef]
36. Jatiault, R.; Dhont, D.; Loncke, L.; Durrieu de Madron, X.; Dubucq, D.; Channelliere, C.; Bourrin, F. Deflection of natural oil droplets through the water column in deep-water environments: The case of the Lower Congo Basin. *Deep-Sea Res. Part I* **2018**, *136*, 44–61. [CrossRef]
37. Jauer, C.D.; Budkewitsch, P. Old marine seismic and new satellite radar data: Petroleum exploration of north west Labrador Sea, Canada. *Mar. Pet. Geol.* **2010**, *27*, 1379–1394. [CrossRef]

38. Leifer, I.; Boles, J.R.; Luyendyk, B.P.; Clark, J.F. Transient discharges from marine hydrocarbon seeps: Spatial and temporal variability. *Environ. Geol.* **2004**, *46*, 1038–1052. [CrossRef]
39. Liira, M.; Noormets, R.; Sepp, H.; Kekišev, O.; Maddison, M.; Snorre, O. Sediment geochemical study of hydrocarbon seeps in Isfjorden and Mohnbukta: A comparison between western and eastern Spitsbergen, Svalbard. *Arktos* **2019**, *5*, 49–62. [CrossRef]
40. Logan, G.A.; Jones, A.T.; Kennard, J.M.; Ryan, G.J.; Rollet, N. Australian offshore natural hydrocarbon seepage studies, a review and re-evaluation. *Mar. Pet. Geol.* **2010**, *27*, 26–45. [CrossRef]
41. Mitra, D.S.; Majumdar, T.J.; Ramakrishan, R.; Dave, H.; Mazumder, S. Detection and monitoring of offshore oil seeps using ERS/ENVISAT SAR/ASAR data and seep-seismic studies in Krishna–Godavari offshore basin, India. *Geocarto Int.* **2013**, *28*, 404–419. [CrossRef]
42. Mityagina, M.; Lavrova, O. Oil slicks from natural hydrocarbon seeps in the South-Eastern Black Sea, their drift and fate as observed via remote sensing. In Proceedings of the IGARSS 2018—2018 IEEE International Geoscience and Remote Sensing Symposium, Valencia, Spain, 22–27 July 2018; pp. 7926–7929.
43. Nemirovskaya, I.A.; Sivkov, V.V. Peculiarities in the distribution of hydrocarbons in the southeastern part of the Baltic Sea. *Oceanology* **2012**, *52*, 34–47. [CrossRef]
44. Nesbitt, E.A.; Martin, R.A.; Campbell, K.A. New records of Oligocene diffuse hydrocarbon seeps, northern Cascadia margin. *Palaeogeogr. Palaeoclimatol. Palaeoecol.* **2013**, *390*, 116–129. [CrossRef]
45. Pinet, N.; Duchesne, M.; Lavoie, D.; Bolduc, A.; Long, B. Surface and subsurface signatures of gas seepage in the St. Lawrence Estuary (Canada): Significance to hydrocarbon exploration. *Mar. Pet. Geol.* **2008**, *25*, 271–288. [CrossRef]
46. Römer, M.; Sahling, H.; Pape, T.; Bohrmann, G.; Spieß, V. Quantification of gas bubble emissions from submarine hydrocarbon seeps at the Makran continental margin (offshore Pakistan). *J. Geophys. Res.* **2012**, *117*, C10015. [CrossRef]
47. Römer, M.; Sahling, H.; Pape, T.; dos Santos Ferreira, C.; Wenzhöfer, F.; Boetius, A.; Bohrmann, G. Methane fluxes and carbonate deposits at a cold seep area of the Central Nile Deep Sea Fan, Eastern Mediterranean Sea. *Mar. Geol.* **2014**, *347*, 27–42. [CrossRef]
48. Sakran, S.; Nabih, M.; Henaish, A.; Ziko, A. Structural regime and its impact on the mechanism and migration pathways of hydrocarbon seepage in the southern Gulf of Suez rift: An approach for finding new unexplored fault blocks. *Mar. Pet. Geol.* **2016**, *71*, 55–75. [CrossRef]
49. Short, J.W.; Kolak, J.J.; Payne, J.R.; Van Kooten, G.K. An evaluation of petrogenic hydrocarbons in northern Gulf of Alaska continental shelf sediments—The role of coastal oil seep inputs. *Org. Geochem.* **2007**, *38*, 643–670. [CrossRef]
50. Taylor, M.H.; Dillon, W.P.; Pecher, I.A. Trapping and migration of methane associated with the gas hydrate stability zone at the Blake Ridge Diapir: New insights from seismic data. *Mar. Geol.* **2000**, *164*, 79–89. [CrossRef]
51. Venkatesan, M.I.; Naidu, A.S.; Blanchard, A.L.; Misra, D.; Kelley, J.J. Historical changes in trace metals and hydrocarbons in nearshore sediments, Alaskan Beaufort Sea, prior and subsequent to petroleum-related industrial development: Part II. Hydrocarbons. *Mar. Pollut. Bull.* **2013**, *77*, 147–164. [CrossRef]
52. Zakharenko, A.S.; Galachyants, Y.P.; Morozov, I.V.; Shubenkova, O.V.; Morozov, A.A.; Ivanov, V.G.; Pimenov, N.V.; Krasnopeev, A.Y.; Zemskaya, T.I. Bacterial Communities in Areas of Oil and Methane Seeps in Pelagic of Lake Baikal. *Microb. Ecol.* **2019**, *78*, 269–285. [CrossRef]
53. Zelilidis, A.; Maravelis, A.G.; Tserolas, P.; Konstantopoulos, P.A. An overview of the petroleum systems in the Ionian Zone, onshore NW Greece and Albania. *J. Pet. Geol.* **2015**, *38*, 331–348. [CrossRef]
54. N.O.A.A. Emergency Response Division. Open Water Oil Identification Job Aid for Aerial Observation. 2016. Available online: https://response.restoration.noaa.gov/oil-and-chemical-spills/oil-spills/resources/open-water-oil-identification-job-aid.html (accessed on 28 May 2022).
55. Brekke, C.; Solberg, A.H.S. Oil spill detection by satellite remote sensing. *Remote Sens. Environ.* **2005**, *95*, 1–13. [CrossRef]
56. Leifer, I.; Lehr, W.J.; Simecek-Beatty, D.; Bradley, E.; Clark, R.; Dennison, P.; Hu, Y.; Matheson, S.; Jones, C.E.; Holt, B.; et al. State of the art satellite and airborne marine oil spill remote sensing: Application to the BP Deepwater Horizon oil spill. *Remote Sens. Environ.* **2012**, *124*, 185–209. [CrossRef]
57. Fingas, M.; Brown, C.E. A review of oil spill remote sensing. *Sensors* **2018**, *18*, 906–950.
58. Daneshgar Asl, S.; Dukhovskoy, D.S.; Bourassa, M.; MacDonald, I.R. Hindcast modeling of oil slick persistence from natural seeps. *Remote Sens. Environ.* **2017**, *189*, 96–107. [CrossRef]
59. Razaz, M.; Di Iorio, D.; Wang, B.; Daneshgar Asl, S.; Thurnherr, A.M. Variability of a natural hydrocarbon seep and its connection to the ocean surface. *Sci. Rep.* **2020**, *10*, 12654. [CrossRef] [PubMed]
60. Garcia-Pineda, O.; Zimmer, B.; Howard, M.; Pichel, W.; Li, X.; MacDonald, I.R. Using SAR images to delineate ocean oil slicks with a texture-classifying neural network algorithm (TCNNA). *Can. J. Remote Sens.* **2009**, *35*, 411–421. [CrossRef]
61. Garcia-Pineda, O.; Holmes, J.; Rissing, M.; Jones, R.; Wobus, C.; Svejkovsky, J.; Hess, M. Detection of oil near shorelines during the Deepwater Horizon oil spill using synthetic aperture radar (SAR). *Remote Sens.* **2017**, *9*, 567. [CrossRef]
62. Meng, T.; Yang, X.; Chen, K.-S.; Nunziata, F.; Xie, D.; Buono, A. Radar backscattering over sea surface oil emulsions: Simulation and observation. *IEEE Trans. Geosci. Remote Sens.* **2022**, *60*, 1–14. [CrossRef]
63. Nunziata, F.; de Macedo, C.R.; Buono, A.; Velotto, D.; Migliaccio, M. On the analysis of a time series of X-band TerraSAR-X SAR imagery over oil seepages. *Int. J. Remote Sens.* **2018**, *40*, 3623–3646. [CrossRef]
64. De Beukelaer, S.M.; MacDonald, I.R.; Guinnasso, N.L., Jr.; Murray, J.A. Distinct side-scan sonar, RADARSAT SAR, and acoustic profiler signatures of gas and oil seeps on the Gulf of Mexico slope. *Geo-Mar. Lett.* **2003**, *23*, 177–186. [CrossRef]

65. Abrams, M.A.; Logan, G. Geochemical evaluation of ocean surface slick methods to ground truth satellite seepage anomalies for seepage detection. In Proceedings of the Annual Meeting—American Association of Petroleum Geologists: Unmasking the Potential of Exploration & Production, New Orleans, LA, USA, 11–14 April 2010.
66. MacDonald, I.R.; Leifer, I.; Sassen, R.; Stine, P.; Mitchell, R.; Guinasso, N., Jr. Transfer of hydrocarbons from natural seeps to the water column. *Geofluids* **2002**, *2*, 95–107. [CrossRef]
67. Johansen, C.; Macelloni, L.; Natter, M.; Silva, M.; Woosley, M.; Woolsey, A.; Diercks, A.R.; Hill, J.; Viso, R.; Marty, E.; et al. Hydrocarbon migration pathway and methane budget for a Gulf of Mexico natural seep site: Green Canyon 600. *Earth Planet. Sci. Lett.* **2020**, *545*, 116411. [CrossRef]
68. Abrams, M.A. Distribution of subsurface hydrocarbon seepage in near-surface marine sediments. In *Hydrocarbon Migration and Its Near-Surface Expression*; Schumacher, D., Abrams, M.A., Eds.; AAPG Memoir 66; American Association of Petroleum Geologists: Tulsa, OK, USA, 1996; pp. 1–14.
69. Jatiault, R.; Dhont, D.; Loncke, L.; Dubucq, D. Monitoring of natural oil seepage in the Lower Congo Basin using SAR observations. *Remote Sens. Environ.* **2017**, *191*, 258–272. [CrossRef]
70. Jones, A.T.; Logan, G.A.; Kennard, J.M.; Rollet, N. Reassessing potential origins of synthetic aperture radar (SAR) slicks from the Timor Region of the North West Shelf on the basis of field and ancillary data. *Appea J.* **2005**, *45*, 311–331. [CrossRef]
71. Jones, A.T.; Thankappan, M.; Logan, G.A.; Kennard, J.M.; Smith, C.J.; Williams, A.K.; Lawrence, G.M. Coral spawn and bathymetric slicks in synthetic aperture radar (SAR) data from the Timor Sea, north-west Australia. *Int. J. Remote Sens.* **2006**, *27*, 2063–2069. [CrossRef]
72. Wu, L.; Wang, L.; Min, L.; Hou, W.; Guo, Z.; Zhao, J.; Li, N. Discrimination of algal-bloom using spaceborne SAR observations of Great Lakes in China. *Remote Sens.* **2018**, *10*, 767. [CrossRef]
73. Environmental Systems Research Institute. Aggregate Points. Available online: https://doc.arcgis.com/en/arcgis-online/analyze/aggregate-points.htm#:~{}:text=The%20Aggregate%20Points%20tool%20uses,each%20area%20using%20graduated%20symbols (accessed on 18 May 2022).
74. Leifer, I.; Boles, J. Measurement of marine hydrocarbon seep flow through fractured rock and unconsolidated sediment. *Mar. Pet. Geol.* **2005**, *22*, 551–568. [CrossRef]
75. B.O.E.M. Seismic Water Bottom Anomalies Map Gallery. Available online: https://www.boem.gov/oil-gas-energy/mapping-and-data/map-gallery/seismic-water-bottom-anomalies-map-gallery (accessed on 25 February 2000).
76. B.O.E.M. Northern GoM Deepwater Bathymetry Grid from 3D Seismic. Available online: https://www.boem.gov/oil-gas-energy/mapping-and-data/map-gallery/northern-gom-deepwater-bathymetry-grid-3d-seismic (accessed on 25 March 2022).
77. Leifer, I.; Boles, J. Turbine tent measurements of marine hydrocarbon seeps on subhourly timescales. *J. Geophys. Res.* **2005**, *110*, C01006. [CrossRef]
78. Quigley, D.C.; Hornafius, J.S.; Luyendyk, B.P.; Francis, R.D.; Clark, J.; Washburn, L. Decrease in natural marine hydrocarbon seepage near Coal Oil Point, California, associated with offshore oil production. *Geology* **1999**, *27*, 1047–1050. [CrossRef]
79. Leifer, I. A Synthesis Review of Emissions and Fates for the Coal Oil Point Marine Hydrocarbon Seep Field and California Marine Seepage. *Geofluids* **2019**, *2019*, 4724587. [CrossRef]
80. U.S. EIA. Petroleum & Other Liquids. Available online: https://www.eia.gov/dnav/pet/hist/LeafHandler.ashx?n=pet&s=mcrfp3fm2&f=a (accessed on 2 June 2021).